Association of Metallurgical Engineers of Serbia *Scientific paper*
AMES *UDC: 669.131.7:621.193.16*

THE MORPHOLOGY OF DUCTILE CAST IRON SURFACE DAMAGED BY CAVITATION

Marina Dojčinović[1*], Olivera Erić[2], Dragan Rajnović[3], Leposava Sidjanin[3], Sebastijan Baloš[3]

[1] *University of Belgrade, Faculty of Technology and Metallurgy, Karnegijeva 4, Belgrade, Serbia, e-mail: rina @tmf.bg.ac.rs*
[2] *Institute 'Kirilo Savic', Belgrade, Serbia*
[3] *Department of Production Engineering, Faculty of Technical Sciences, University of Novi Sad, Novi Sad, Serbia*

Received 15.11.2011
Accepted 15.01.2012

Abstract

The study was designed to investigate the cavitation behavior of the ductile cast iron with microstructure consisting of spheroidal graphite in a predominantly ferrite matrix with 10% pearlite. The experiments were conducted using the ultrasonically induced cavitation test method. The frequency of vibration and the peak-to-peak displacement amplitude of the horn were 20±0.5 kHz and 50μm, respectively, with separation of 0.5 mm between the sample and the horn tip. In order to obtain the erosion curve, the mass loss measurements were performed after each exposure interval. The mass loss was recorded every 30min for a test period of 240 min. Roughness parameter Ra (the mean roughness), was used to characterize the surfaces. The cavitation rate was 1.85 higher for ductile iron compared with that of carbon steel with similar hardness, because graphite removal produces high stress concentration in cast iron. Compared with conventional mass loss measurements in assessing material degradation in cavitation erosion, surface roughness measurements provide an alternative and convenient method.

Key words: Ductile cast iron, cavitation, morphology, graphite, roughness

Introduction

Cavitation phenomen, characterized by the generation and the collapse of vapor structure in liquid, frequently occurs in hydraulic machinery parts [1,2]. The shock waves and microjets emitted during the collapses of vapor structures interact with neighboring solid surfaces may cause the material damage [3-5].

[*] Corresponding author: Marina Dojčinović, rina@tmf.bg.ac.rs

The cavitation erosion resistance of a material is commonly determined by mass loss measurements in the laboratory using an ultrasonic vibratory apparatus and the resistance is reported in term cavitation rate. Methods alternative to mass loss-time measurements to quantify erosion damage represent evoluation of surface roughness parameters which provide more detailed information in addition to erosion loss [6,7].

Cavitation investigations proved that cavitation resistance of conventional materials such as ferrous alloys commonly used in production of hydraulic machinery parts, depends on mechanical properties (hardness, tensile strength) and microstructure [8]. Heymann summarized that the correlation between cavitation resistance and hardness was more accurate when compared with the other mechanical properties for many ferrous and non-ferrous alloys [9]. Hattory and Kitagawa [10] presented reviews including the erosion resistance of various kinds of cast iron, i.e gray cast iron, ductile cast iron FCD400 and FCD700, ferrite phase ductile cast iron FDI, pearlite phase ductile cast iron PDI and austempered ductile iron ADI. The erosion resistance was 1/3 to 1/5 lower for gray cast iron and 2/3 to 1/3 lower for ductile cast iron compared with that of carbon steel with the same hardness. The reason for such a behavior may be ascribed to graphite removal producing high stress concentrations for cast iron.

The literature survey shows that numerous scientific researches have been done on the grey and austempered ductile iron, but only few on nodular cast iron with ferrite matrix may be found [11]. A small number of studies have been performed on the effect of microstructure with a wide variety of ferrite/pearlite ratios on cavitation resistance behavior of ductile cast iron.

Therefore, the aim of this work was to study the cavitation behavior of ductile cast iron with microstructure consisting of spheroidal graphite in a predominantly ferrite matrix with 10% pearlite and to compare cavitation with carbon steel of similar hardness.

Experimental

Materials

In this paper, for laboratory testing of cavitation resistance unalloyed ferritic ductile cast iron was used.

The chemical composition (in wt.%) of ductile cast iron was as follows: 3.53 C, 2.53 Si, 0.347 Mn, 0.045 Cu, 0.069 Ni, 0.055 Cr, 0.031 Mg and the rest was Fe.

Ductile cast iron was produced by a sandwich spheroidization treatment (i.e., the melt was poured into the green sand moulds, and 25-mm-thick Y block castings were obtained). Base irons were treated with 2.2 wt.% MgFeSi alloy for spheroidization followed by postinoculation with 75 wt.% FeSi.

Methods

Standard metallographic preparation techniques (the wafer specimens cut from Y-block castings were etched in 3% nital solution after grinding and polishing) were applied prior to light microscopy (LM) investigation.

Vickers hardness tests on the cross sections of the test specimens were also performed in order to verify the existence of work-hardened subsurface layers affected by cavitation. For all specimens Vickers hardness (HV30, ISO 6507-1) was determined at room temperature.

Detailed morphological examinations were made on all specimens tested under cavitation conditions using light microscopy (LM) and scanning electron microscopy (SEM).

The cavitation test was performed using an ultrasonic equipment [12,13]. The frequency of vibration and the peak-to-peak displacement amplitude of the horn were 20±0.5 kHz and 50μm, respectively, with separation of 0.5mm between the specimens and the horn tip. The test liquid was water maintained at 25±0.5°C.

Prior to test, all specimens were ground and polished in order to obtain surface with initial mean roughness Ra lower than 0.05 μm. In order to obtain the erosion curve, the mass loss measurements were performed after each exposure interval. Before the test and after each test interval the specimens were cleaned and dried with hot air. The mass loss was recorded every 30min for a test period of 240 min. Mass losses of the tested specimens were measured using an analytical balance with an accuracy of ±0.1 mg.

The evaluation of surface roughness in ultrasonic cavitation tests was monitored using profilometric measurements by TR200 Surface Roughness Tester [14]. The measurement results were recorded using Software TR200 Time Data View. Measured parameter of the mean roughness Ra representing arithmetic mean of the absolute values of surface profile deviations (Yi) of the center line + 1 is given by the equation 1:

$$R_a = \frac{1}{n}\sum_{i=1}^{n} |y_i| \qquad (1)$$

Results and discussion

The morphology of graphite nodules in the microstructure of ductile iron (Fig. 1a) and (Fig. 1b) is fully spherical with the nodule count from 60 to 80 nodule/m^2. The spheroidization is evident more than 90% with an average nodule size varying between 35 and 55μm. The microstructure of ductile iron after polishing and etching consisted of spheroidal graphite in a predominantly ferrite matrix with 10% pearlite (Fig. 1b).

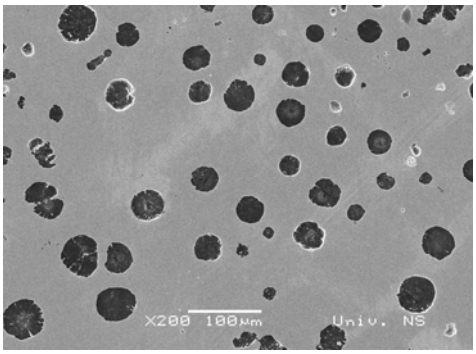

Fig. 1a. SEM micrograph. Size, shape and distribution of graphite nodules in as-cast ductile iron, unetched.

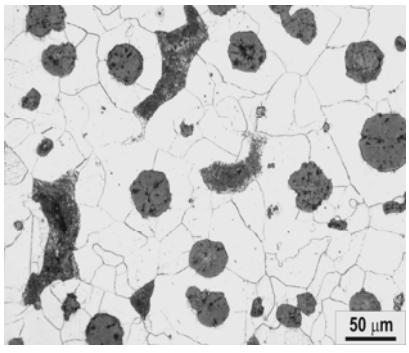

Fig. 1b. Light micrograph. Microstructure of ductile cast iron, etched.

SEM micrographs of ductile iron after cavitation testing in water are shown in Fig. 2.

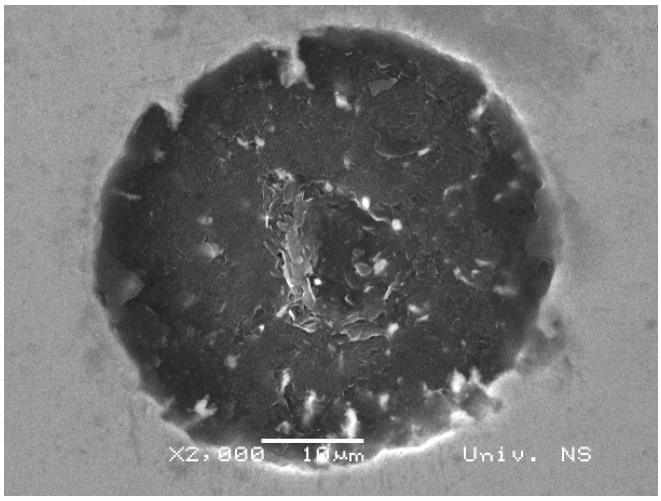

Fig. 2 SEM micrograph. The partially fragmented ***graphite nodule.***

At the beginning of cavitation testing the separation of graphite nodules from ferrite matrix occurs. Figure 2 shows the detail of this separation.

With increase of testing time cavitation caused the separation of graphite nodules from ferrite matrix leaving pits (Fig. 3). The portion remaining after the nodules removal has the form of pits with notchs with high stress concentration and representing favorable locations for cavitation erosion. In the initial periods ferrite matrix was slightly attacked.

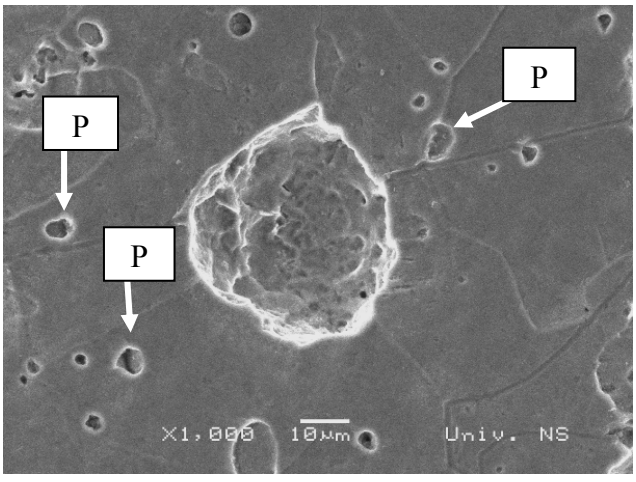

Fig. 3 SEM micrograph. Pits produced by graphite nodule removal. P-pits.

Cavitation bubbles collapse and induce a microjet, which may instantaneously produce intense local heating and high pressure [15]. Cavitation erosion is produced by the impulsive pressure, which is generated from the collapse of cavitation bubbles either at or near the solid surface. The total energy of cavitation clouds is transferred to the solid material and must be either absorbed or dissipated by the solid or reflected as shock waves in the liquid. Solid material absorbs the impact energy conducting elastic deformation, plastic deformation, or fracture.

When the ductile material is exposed to cavitation, local plastic deformation of its surface is observed. This deformation is in the form of surface undulations with the appearance of defects, such as grain boundaries and slip bands. With time, these undulation changes in width and height, but generally they do not change in shape and number [16].

Implosion of collapsing cavitation bubbles in the solid surface of ferrite matrix caused plastic deformation in the form of micropits on the location of defects. Their average size was about 3 μm in diameter. With an increase in the number of collapsing bubbles the number of micropits also increases, and the solid surface undergoes undulation (Fig. 4).

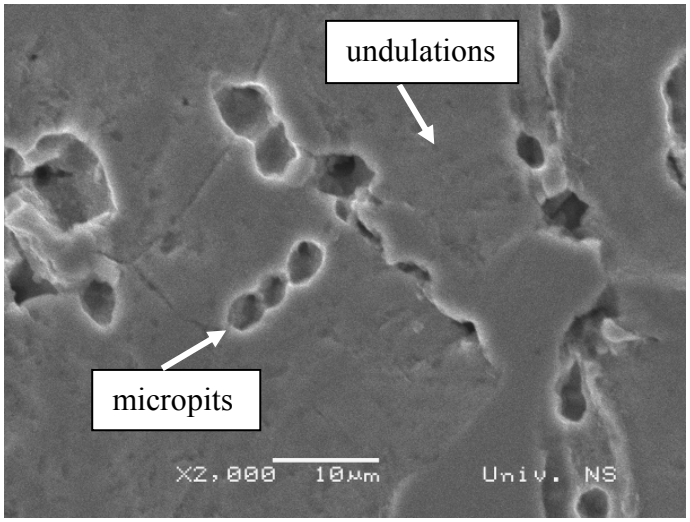

Fig. 4 SEM micrograph. Micropits on the location of defects

Fatigue cracks may nucleate at various sites of the test surface such as polishing line traces, micropits, grain boundaries, small defects in the material and microstructural discontinuities formed by plastic deformation. These sites represent origin of stress concentration. The pits formed along the location of defects coalesce and form a microcrack (Fig. 5).

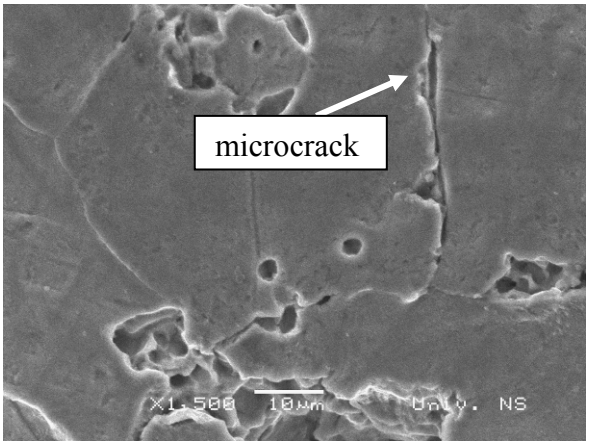

Fig. 5 SEM micrograph. Formation of a microcrack by coalescence of pits.

Fatigue crack which develop around the pit formed by graphite nodule removal. This crack causes the separation of the large particle of ferrite matrix shown in Fig. 6.

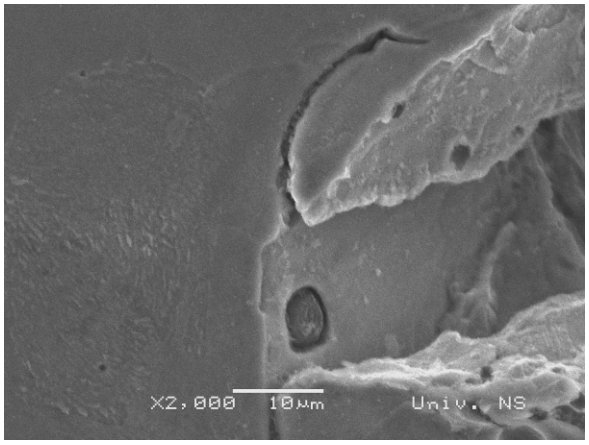

Fig. 6 SEM micrograph. The crack formed around pit of removed nodule.

Undulations are formed on grain boundaries and slip bands. Figs. 7 and 8 show the morphology and degree of undulations for different time interval of cavitation testing. More undulations appear with longer time of testing.

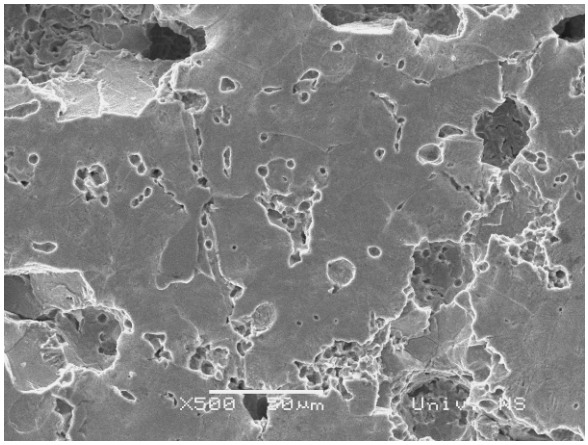

Fig. 7 SEM micrograph of ductile iron after cavitation testing in water (60min). The eroded surface.

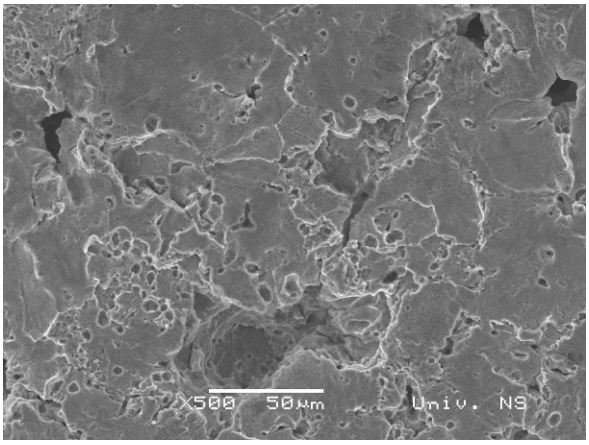

Fig. 8 SEM micrograph of ductile iron after cavitation testing in water (120min). The eroded surface.

With increasing time of testing the attacked area of the specimen became larger with more pits, micropits and surface deformation. Ductile deformation can also spread to the matrix away from the pits that formed as a result of the removal of graphite nodules. The ductile removal of the material in the matrix by coalescence of these pits with formation of deep craters was observed in Fig. 9. Fatigue becomes a major degradation mechanism and wear particles are detached when several microcracks join and grow together.

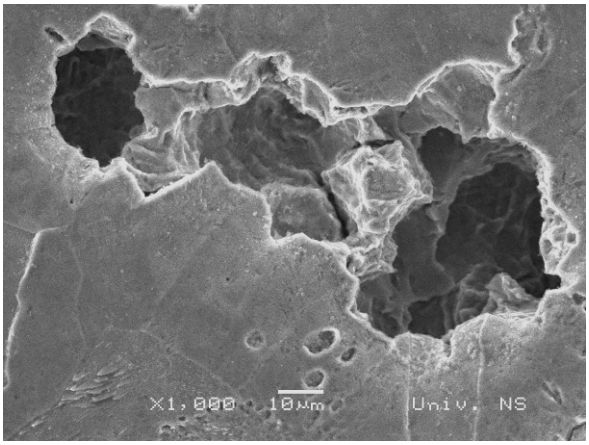

Fig. 9 SEM microgsraph. Removal of material of the ferrite matrix by coalescence of pits.

Simultaneously with cavitation damage of ferrite, on the bottom of pits caused by the separation of graphite a presence of microtunnel may be seen. The formation of microtunnel was probably caused by microjetting degradation (Fig. 10).

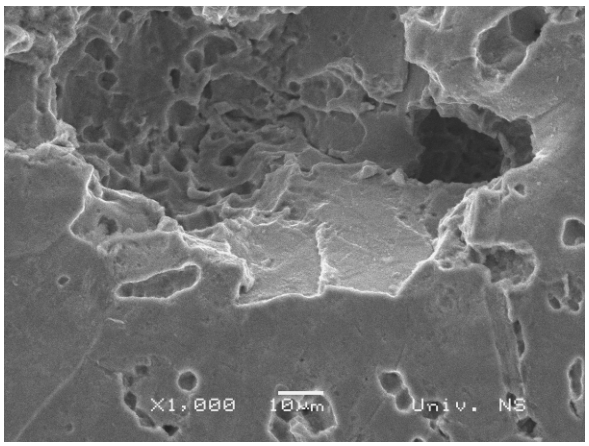

Fig. 10 SEM micrograph. Microtunnel caused by microjet

As the shock waves continue to hit the surface during the acceleration stage a number of craters are formed with heavily strained material around them. In this situation fatigue becomes a major degradation mechanism and wear particles are detached when several microcracks join and grow together (Fig. 11).

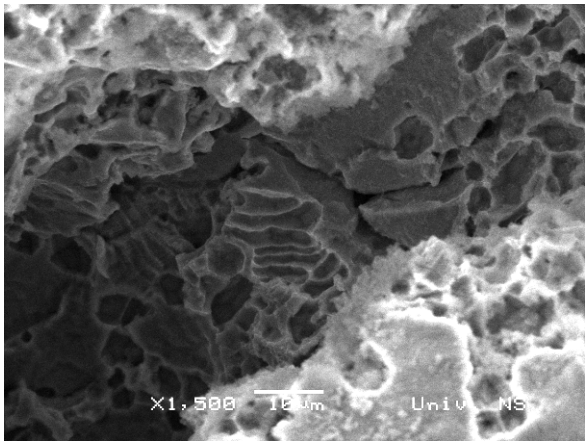

Fig. 11 SEM micrograph. Fatigue slip system.

Consequently, after 240min of testing numerous craters and grooves with intense plastic deformation can be observed on the damaged surface (Fig. 12). At high magnifications, slip lines were observed in the ferritic matrix, with microvoids developing at emerging slip steps (Fig. 13).

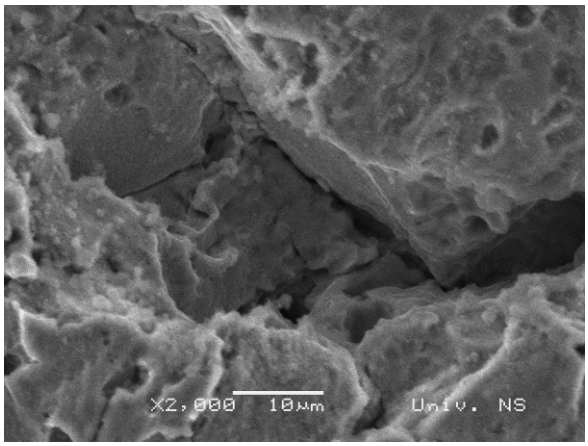

Fig. 12 SEM micrograph. Fatigue microcracks and microtunnel.

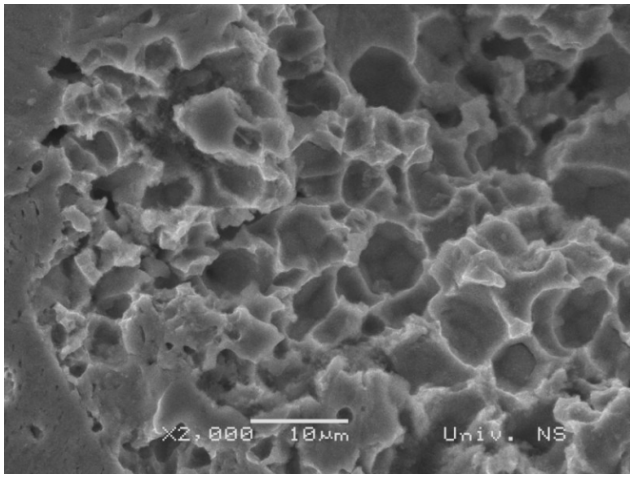

Fig. 13 SEM micrograph of ductile iron after cavitation testing for 240min. Groves and microvoids are formed along the phase boundaries after cavitation.

The diagram in Fig. 14 shows relation between mass loss and testing time, where the line was drawn by the least-square method and data can be expressed by a straight line. The slope of the straight line represents the cavitation rate. The calculated slope for ductile cast iron corresponds to the cavitation rate of 0.118 mg/min. The coefficient of correlation calculated by regression analysis is R^2=0.9878.

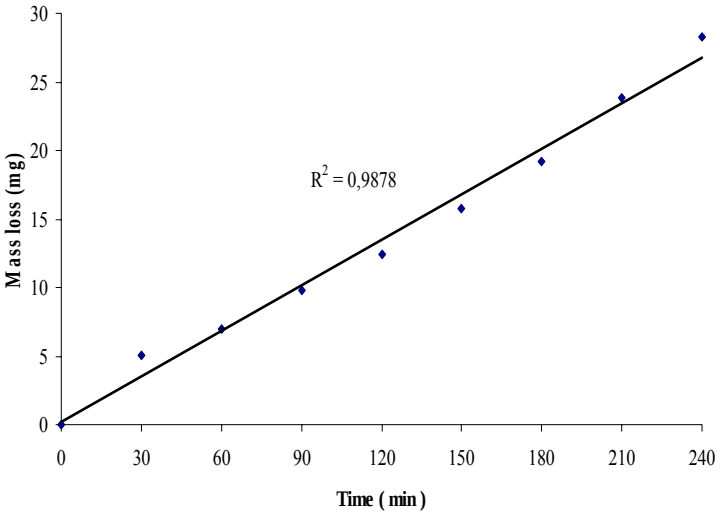

Fig. 14. Rate of cavitation erosion of the ductile cast iron.

The morphology of the cavitation damage of heat treated medium carbon steel was analyzed and the measured hardness was 187 HV, whereas cavitation rate was 0.0639 mg/min [15]. The measured hardness of ductile cast iron, which was tested in this paper was 168 HV and cavitation rate was 0.1179 mg/min. Thus, the cavitation rate of ductile cast iron is 1.85 times higher compared with that of carbon steel of the similar hardness, because graphite removal produces high stress concentrations in cast iron.

The mean surface roughness Ra of ductile cast iron exposed to cavitation during the testing time was given in Fig.15.

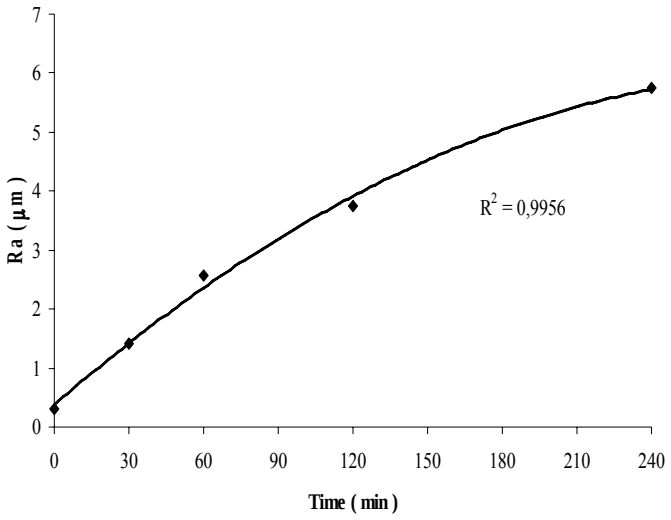

Fig. 15 Changes in surface roughness parameter Ra during testing time.

The roughness of ductile cast iron was changed from Ra=0.05µm before the test to Ra=5.749µm at the end of the test. The less increase of surface roughness was observed in early stages of the cavitation test (30 and 60min) as a result of graphite nodules removal. In subsequent stages (120 and 240min) of test damage of the matrix appears leading to the significant increase of surface roughness. The coefficient of correlation R^2=0.9956 of roughness measurements is in very good agreement with that of R^2=0.9878 corresponding to mass loss measurements.

Conclusions

According to the analysis of experimental results, morphological observations via SEM can be summarized as follows:

- Cavitation erosion of ductile cast iron begins by removal of graphite nodules and afterwards by ductile removal of material in the ferrite matrix.
- The cavitation rate of ductile cast iron was 1.85 higher compared with that of carbon steel with similar hardness, because graphite removal produces in cast iron high stress concentration.

- Compared with conventional mass loss measurements in assessing material degradation in cavitation erosion, surface roughness measurements provide an alternative and convenient method.

Acknowledgements

The authors are indebted to the Ministry of Education and Science of the Republic of Serbia for the financial support of the project TR34015.

References

[1] R.T. Knapp, J.W. Daily, F.G. Hammit, Cavitation, McGraw-Hill, New York, 1970.
[2] T. Okada, Y. Iwai, S. Hattory, N. Tanimura, Wear 184 (1994) 231.
[3] S. Hattori, H. Mori, T. Okada, J. Fluid Eng., Trans. ASME 120 (1998) 179.
[4] T. Okada, S. Hattori, Proc. of the Int. Symposium on Aerospace and Fluid Science, Sendai, Japan, 1993, p. 347.
[5] K. Steller, Proc. of the 6th Int. Conf. on Erosion by Liquid and Solid Impact, Cambridge, UK, 1983, p. 121.
[6] A.Karimi, J.L.Martin, Int.Met.Rev.31 (1) (1986) 1-26.
[7] K.Y.Chiu, F.T.Cheng, H.C. Man, Ultrasonic 43 (2005) 713-716.
[8] F.G. Hammit, Cavitation and Multiphase Flow Phenomena, McGraw-Hill, New York, 1980.
[9] F.J.Heymann, Characterisation and Determination of Erosion Resistance, ASTM STP474, American Society for Testing and Materials, 1970, pp.212-222.
[10] S.Hattori, T. Kitagawa, Wear 269 (2010) 443-448.
[11] K.F. Alabeedia, J.H. Abbouda, K.Y. Benyounisb, Wear 266 (2009) 925–933.
[12] ASTM Standard G32-92, Annual Book of ASTM Standards, vol. 03.02, ASTM, Philadelphia, 1992.
[13] M.Dojčinović, Ph.D.Thesis, University of Belgrade, 2007.
[14] M.M. Bučko, S.I. Stevanović., M.V. Tomić, M.G. Pavlović, J.B. Bajat, Hem. Ind. 65 (2011) 295-303. Chemical Industry, (2011) DOI:10.2298/HEMIND 101214003B.
[15] M. Dojčinović, S. Marković, J. Serb. Chem. Soc. 71 (8-9) (2006) 977-984.
[16] M. Dojčinović, T. Volkov-Husović, Mater. Lett. 62 (2008) 953-956.